


Cite this: *RSC Adv.*, 2021, 11, 32965

# One-pot synthesis of Ag–Cu–Cu<sub>2</sub>O/C nanocomposites derived from a metal–organic framework as a photocatalyst for borylation of aryl halide†

Dicky Annas,<sup>a</sup> Shamim Ahmed Hira,<sup>a</sup> Sehwan Song,<sup>b</sup> Jong-Seong Bae,<sup>c</sup> Sungkyun Park<sup>b</sup> and Kang Hyun Park<sup>ib</sup>\*<sup>ad</sup>

Mixed metal–metal oxide/C (Ag–Cu–Cu<sub>2</sub>O/C) nanocomposites were synthesized by the heat treatment of a metal–organic framework under a N<sub>2</sub> flow using the one-pot synthesis method. The as-prepared nanocomposites were characterized using a range of techniques, such as TEM, elemental mapping, XRD, N<sub>2</sub> sorption, UV-Vis DRS, and XPS. The nanoparticles were successfully formed with high dispersion in porous carbon materials and high crystallinity based on the analysis results. The Ag–Cu–Cu<sub>2</sub>O/C nanocomposites (35 nm) showed high photocatalytic activity and good recyclability toward the borylation of aryl halides under a xenon arc lamp. This result can enhance the interest in photocatalysis for various applications, particularly in organic reactions, using a simple and efficient synthesis method.

Received 21st July 2021  
Accepted 17th September 2021

DOI: 10.1039/d1ra05586k

rsc.li/rsc-advances

## Introduction

Metal and metal oxide nanocomposites can be tuned to obtain a range of properties for various applications, such as catalysis. The performance of nanocomposites and nanostructured systems can be improved through interactions between two or more materials.<sup>1,2</sup> Compared to single metals or metal oxides, these nanocomposites have unique properties, such as stability, selectivity, and good electronic and optical properties.<sup>3–5</sup> Nanocomposites are effective structures for photocatalytic applications because of their high photoelectron–hole separation. When nanocomposites between two or more materials with matching band potentials are formed, heterojunction interfaces are also formed, which play important roles in separating photoproduced electron–hole pairs.<sup>6–8</sup>

Support materials, such as carbon, zeolites, graphene, silica, and metal–organic frameworks, are used to load the metal and metal oxides nanocomposites in their surface to produce a heterogeneous catalyst. These support materials minimize aggregation between materials and increase stability when used as a catalyst in various reactions. Carbon is a commonly used support material because of its high mechanical properties,

high electrical properties, high thermal properties, an high surface area.<sup>9–11</sup> In addition to being used as a support material to increase the catalytic activity, the interactions between carbon and metal or metal oxides nanocomposites are limited to physical interactions between the carbon and the materials, and that there is a synergistic effect when these materials are used in catalytic reactions.<sup>12</sup>

Recently, metal–organic frameworks (MOFs), which are porous materials and contain an organic linker and metal ions or clusters, have attracted considerable attention in various fields, such as gas storage, gas adsorption, drug delivery, sensors, and heterogeneous catalysis.<sup>13–16</sup> These materials provide high surface area, tunable porosities, large pore size, and straightforward synthesis.<sup>17</sup> Although MOFs are used in various fields, they are unstable and tend to collapse during high thermal, resulting in a decrease in catalytic activity.<sup>18</sup> The reduction of metal cations in MOFs to metal nanoparticles and metal oxide nanoparticles can be achieved by thermal reduction and chemical reduction or a combination of both methods.<sup>19,20</sup> As a result, these nanocomposites have good stability and high catalytic activity. In addition, it also generates a synergistic effect between metal/metal oxide and support material.

The Cu<sub>3</sub>(BTC)<sub>2</sub> (BTC = 1,3,5-benzenetricarboxylate) is one of the Cu-MOF classes. Previous reports have shown that the calcination of Cu-MOF resulted in mixed Cu, Cu<sub>2</sub>O, and C under N<sub>2</sub> gas conditions, which showed a high catalytic activity.<sup>12,21</sup> The Cu metal and copper oxide (Cu<sub>2</sub>O and CuO) are important as catalysts in organic reactions. In particular, when a combination of both phases is attached to the support material, the catalytic activity will be higher than their single metal/metal

<sup>a</sup>Department of Chemistry, Pusan National University, Busan, 46241, South Korea. E-mail: chemistry@pusan.ac.kr

<sup>b</sup>Department of Physics, Pusan National University, Busan, 46241, South Korea

<sup>c</sup>Busan Center, Korea Basic Science Institute, Busan 46742, South Korea

<sup>d</sup>SoulDot Co., Ltd, Pusan National University, Busandaehak-ro 63beon-gil, Geumjeong-gu, Busan 46241, Korea

† Electronic supplementary information (ESI) available. See DOI: 10.1039/d1ra05586k



oxide counterparts, especially under visible light.<sup>12</sup> Moreover, the photocatalytic activity under visible light can be enhanced by adding other noble metal nanoparticles, such as Ag nanoparticles, because its surface plasmon resonance (SPR) improves the absorption of visible light.<sup>22–26</sup>

In this study, Ag–Cu–Cu<sub>2</sub>O/C nanocomposites were prepared using a one-pot synthesis method derived from Cu-MOF (Cu<sub>3</sub>(BTC)<sub>2</sub>) under N<sub>2</sub> gas. Through this approach, the nanoparticles have small particles size, not easily to aggregate, and using simple and efficient synthesis method. These nanocomposites were applied as a catalyst in the borylation of aryl halides under visible light irradiation (Scheme 1). This reaction was chosen because it can produce arylboronic esters which are an important class of benchmark reagents with broad utility for organic synthesis. This is because these arylboronic esters have several advantages, such as air stability, easy of handling, having a wide functional group, *etc.* In addition, the chemical structure of arylboronic esters is reported to be used in pharmaceutical fields, such as anticancer, proteasome inhibitor, and antimitotic agent.<sup>27,28</sup> Light irradiation is used in this reaction because it can activate aryl carbon–halogen bond dissociation, mild reaction conditions, and short reaction time.<sup>29–32</sup>

## Experimental

### Chemicals

Copper(II) nitrate hemipentahydrate, ((CuNO<sub>3</sub>)<sub>2</sub>·2.5H<sub>2</sub>O, 98%, Aldrich), silver nitrate (AgNO<sub>3</sub>, 99%, Aldrich), 1,3,5-benzenetricarboxylic acid (H<sub>3</sub>BTC, 98%, Aldrich), sodium borohydride (NaBH<sub>4</sub>, TCI), and organic reagents were used without further purification.

### Synthesis of Ag–Cu–Cu<sub>2</sub>O/C derived from MOF

Ag–Cu–Cu<sub>2</sub>O/C nanocomposites were synthesized from Cu-BTC derived at ambient temperatures. Solution A was prepared by dissolving (CuNO<sub>3</sub>)<sub>2</sub>·2.5H<sub>2</sub>O (6 mmol) in 40 mL of methanol. Solution B was prepared by dissolving H<sub>3</sub>BTC (4 mmol) in 40 mL of methanol in a separate flask. Solution A was added to solution B dropwise with stirring at room temperature. Subsequently, the mixture was stirred for another 30 minutes at ambient temperature. An aqueous AgNO<sub>3</sub> (2 mmol in 5 mL of

H<sub>2</sub>O) solution was then added to the mixture and stirred. After 30 minutes, a sodium borohydride solution (2.4 mmol in 4 mL of methanol) was added to the previous mixture dropwise using a syringe. The mixture was then stirred for one hour and allowed to age for 24 hours under static conditions. The precipitate was washed several times with methanol and dried at 80 °C to obtain Ag–Cu-BTC. The Ag–Cu-BTC was heated to 450 °C at a rate of 3 °C min<sup>−1</sup> under a N<sub>2</sub> atmosphere. The heating process was maintained for one hour to obtain the final material.

### Photocatalytic activity

The photocatalytic activity was examined using the borylation of aryl halide as the test reaction. 4-Iodotoluene (1.2 mmol), bis(pinacolato)diboron (0.6 mmol), catalyst (2 mol%), and base (2 equivalent) were mixed in a round bottom flask. The solvent (5 mL) was then added to the mixture. The mixture was stirred at 40 °C in air and exposed to a xenon arc lamp with an intensity of 200 mW cm<sup>−2</sup> for 6 h. After the reaction, the mixture was diluted with dichloromethane and extracted with a Na<sub>2</sub>CO<sub>3</sub> solution. MgSO<sub>4</sub> was then added to the filtrate, filtered, and the solvent was evaporated. The product yield was determined by gas chromatography-mass spectrometry (GC-MS).

### Recyclability tests

The catalyst was separated from the mixture and washed several times with methanol. The catalyst was then dried in a vacuum oven at 80 °C and reused for seven cycles.

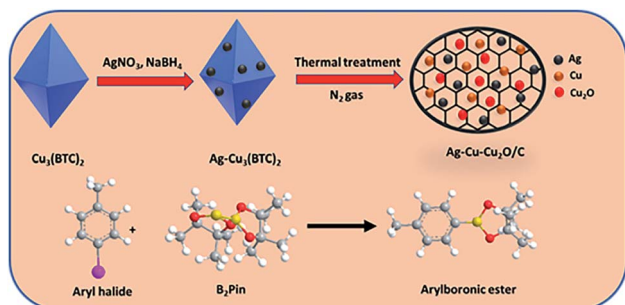
### Material characterization

Transmission electron microscopy (TEM) and elemental mapping by energy-dispersive X-ray spectroscopy (EDS) were carried out using a Talos F200X at 200 kV. The crystal structure was obtained by X-ray diffraction (XRD, Xpert<sup>3</sup>) using Cu-Kα radiation at λ = 0.15406 nm. The N<sub>2</sub> sorption isotherms were analyzed using a Micromeritics ASAP 2020 surface area analyzer at 77 K. Before the analysis, the nanocomposites were degassed at 150 °C for a minimum of 3 h. The chemical properties were analyzed by X-ray photoelectron spectroscopy (XPS, ESCALab250-AXIS SUPRA). The optical properties were conducted using UV-Vis diffuse reflectance spectroscopy (UV-Vis DRS) with V-770 (JASCO Corp., Japan). The photocatalysis experiment products were carried out by GC-MS on a (Shimadzu GC-1010 Plus GCMS-QP2010 SE).

## Results and discussion

### Synthesis of Ag–Cu–Cu<sub>2</sub>O/C nanoparticles

The Ag–Cu–Cu<sub>2</sub>O/C nanoparticles were prepared using copper(II) nitrate hemipentahydrate, 1,3,5-benzenetricarboxylic acid, and silver nitrate as the metal sources with sodium borohydride as the reducing agent through thermal treatment under nitrogen gas flow. The morphology of the nanoparticles were evaluated by TEM. The elemental compositions were evaluated by EDS-mapping. As shown in Fig. 1a, TEM confirmed that the Ag and Cu are transformed to small nanoparticles with



Scheme 1 Brief scheme for the synthesis of the Ag–Cu–Cu<sub>2</sub>O/C nanocomposites as catalyst for borylation of aryl halide.



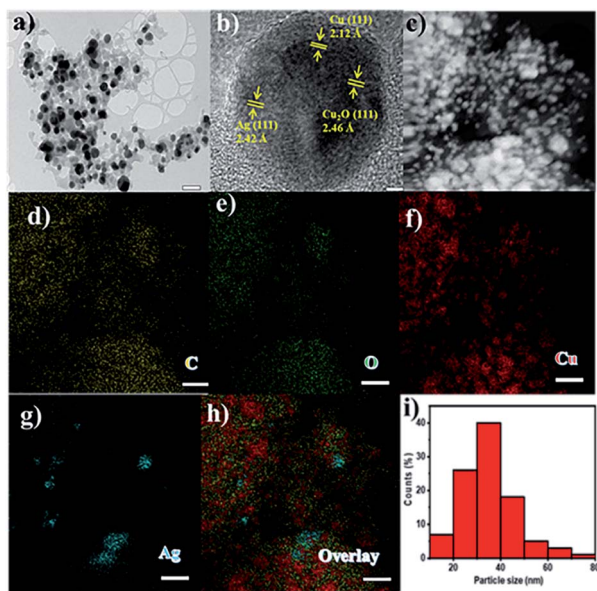


Fig. 1 (a) TEM image, (b) HR-TEM image, (c) HAADF-TEM image, (d–h) elemental mapping images, (i) size distribution histogram of the Ag–Cu–Cu<sub>2</sub>O/C nanocomposites. The bars represent 100 nm (a), 2.5 nm (b), and 200 nm (d–h).

small agglomerates with an average particle size of approximately 35 nm (Fig. 1i). The high-resolution (HR)-TEM images Ag–Cu–Cu<sub>2</sub>O/C nanocomposites in Fig. 1b showed lattice fringe of 2.12 Å, 2.46 Å, and 2.42 Å, which corresponded to the (111) of Cu nanoparticles, the (111) lattice plane of Cu<sub>2</sub>O nanoparticles, and the (111) lattice plane of Ag nanoparticles, respectively. Fig. 1d–h shows the elemental mapping image of the Ag–Cu–Cu<sub>2</sub>O/C nanocomposites. The Ag and Cu were highly dispersed in porous carbon materials.

XRD was used to verify the crystallinity structure of the Ag–Cu–Cu<sub>2</sub>O/C nanocomposites and confirm with the reference data for Ag, Cu, and Cu<sub>2</sub>O. Fig. 2a presents the XRD pattern of Cu-BTC, which confirmed the formation of MOF. Cu–Cu<sub>2</sub>O/C nanocomposites were synthesized for comparison. The XRD pattern of these nanocomposites confirmed the presence of Cu<sub>2</sub>O with XRD peaks at 29.66, 36.58, 42.48, and 61.56° 2θ corresponding to the (110), (111), (200), and (220) planes of Cu<sub>2</sub>O nanoparticles, respectively (JCPDS # 78-2076) and Cu nanoparticles with diffraction peaks at 43.46, 50.58, and 74.27° 2θ, corresponding to the (111), (200) and (220) planes of Cu nanoparticles, respectively (JCPDS # 04-0836). The Ag–Cu–Cu<sub>2</sub>O/C nanocomposites showed a similar XRD pattern with the addition of Ag nanoparticles with peaks at 38.21, 44.38, 64.61, and 77.60° 2θ corresponding to the (111), (200), (220) and (311) planes, respectively (JCPDS # 89-3722) (Fig. 2b). Although the Ag–Cu–Cu<sub>2</sub>O/C nanocomposites had a similar XRD pattern to the Cu–Cu<sub>2</sub>O/C nanocomposites, they had different peak intensities, particularly the Cu<sub>2</sub>O peak intensities. In the Ag–Cu–Cu<sub>2</sub>O/C nanocomposites, the XRD peaks for Cu<sub>2</sub>O had a lower intensity compared to Cu–Cu<sub>2</sub>O/C nanocomposites due to the reduction process when silver was added to the synthesis process, and more Cu nanoparticles were produced.

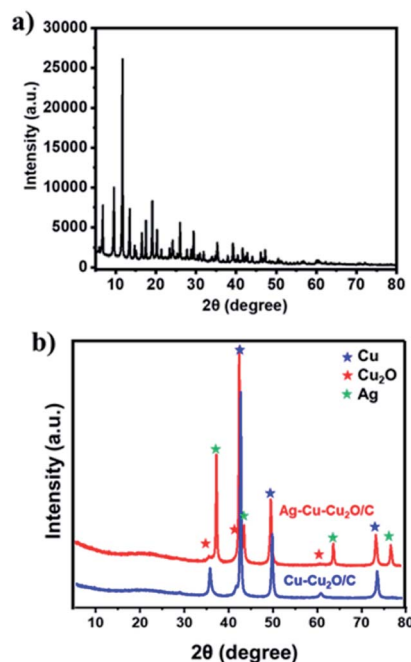


Fig. 2 XRD spectra of (a) Cu<sub>3</sub>(BTC)<sub>2</sub> and (b) as-prepared materials.

The nitrogen adsorption and desorption isotherms of material were conducted using Brunauer–Emmett–Teller (BET) analysis to characterize the porosity of the material. The Ag–Cu–Cu<sub>2</sub>O/C nanocomposites exhibited type IV isotherm, which indicates that a mesoporous structure had formed (Fig. 3a).

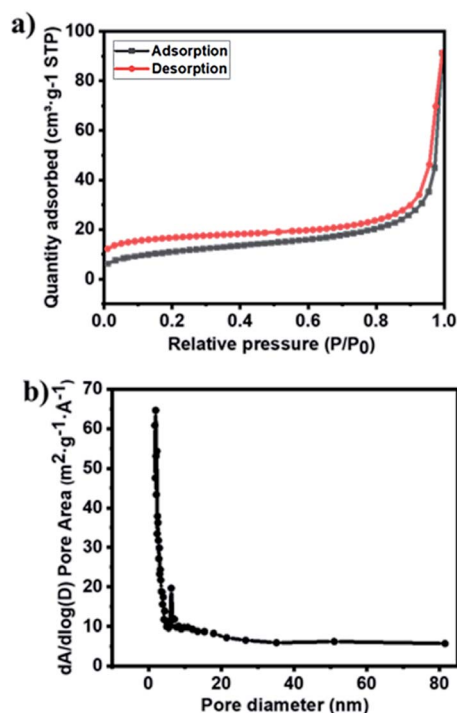


Fig. 3 (a) N<sub>2</sub> isotherms and (b) pore size distribution of Ag–Cu–Cu<sub>2</sub>O/C nanocomposites calculated using the BJH method.



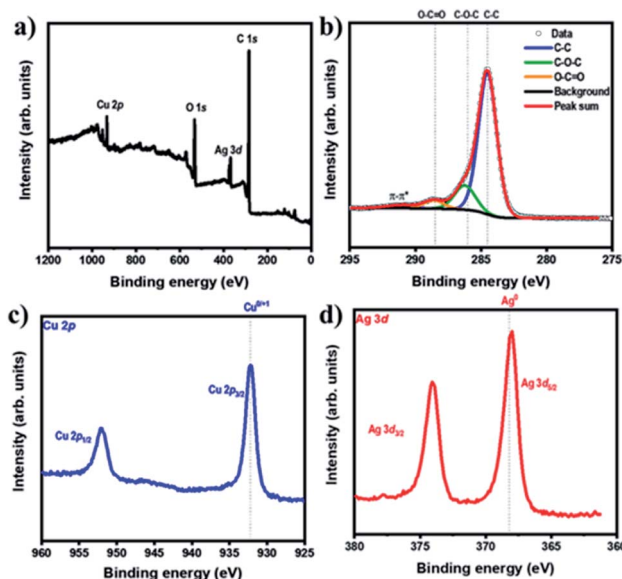


Fig. 4 (a) XPS survey spectra of Ag–Cu–Cu<sub>2</sub>O/C nanocomposites and XPS spectra of (b) C 1s, (c) Cu 2p, and (d) Ag 3d of Ag–Cu–Cu<sub>2</sub>O/C nanocomposites.

From this analysis, the surface area of the material was 39.63 m<sup>2</sup> g<sup>−1</sup>. The average pore size of nanocomposites, which were analyzed using the Barrett–Joyner–Halenda (BJH) method, was 14.25 nm, which was determined from the adsorption and desorption of the isotherm (Fig. 3b).

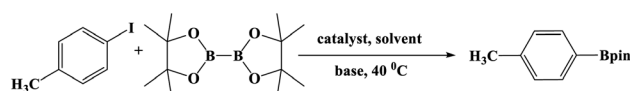
The chemical states and compositions of metal/metal oxides were analyzed by XPS. The XPS survey spectrum in Fig. 4a

revealed Cu, Ag, C, and O in the Ag–Cu–Cu<sub>2</sub>O/C nanocomposites. The Cu 2p XPS spectra of the Ag–Cu–Cu<sub>2</sub>O/C nanocomposites indicated two major peaks at 932.28 eV (2p<sub>3/2</sub>) and 952.08 eV (2p<sub>1/2</sub>). The 2p<sub>3/2</sub> peak confirmed that the copper exists only as Cu<sup>0</sup> and Cu<sup>1+</sup>. No Cu<sup>2+</sup> was observed in the material (Fig. 4c). The Ag 3d peaks appeared at 368.08 eV (3d<sub>5/2</sub>) and 373.97 eV (3d<sub>3/2</sub>). The binding energy of Ag 3d<sub>5/2</sub> peak was consistent with the Ag<sup>0</sup> reference peak (Fig. 4d). These results were well matched with the XRD patterns. In addition, the C 1s XPS spectra were obtained. The deconvolution of the C 1s spectra showed some peaks at 284.50, 286.23, 288.59, and 291.02 eV, which were assigned to C–C, C–O–C, O–C=O, and π–π\*, respectively (Fig. 4b). In addition, the optical properties of nanocomposites were characterized using UV-Vis DRS spectrophotometer. The Ag–Cu–Cu<sub>2</sub>O/C nanocomposites showed a strong absorbance and can absorb the light in the UV to visible region with the calculated band gap of 0.72 eV to excite electrons from the valence band to the conduction band (Fig. 5a).

### Photocatalytic activity of Ag–Cu–Cu<sub>2</sub>O/C

The photocatalytic activity of the Ag–Cu–Cu<sub>2</sub>O/C nanocomposites was examined using the borylation of an aryl halide with 4-iodotoluene and bis(pinacolato)diboron as reactants. To optimize the condition reaction, initially, 1 mol% of Ag–Cu–Cu<sub>2</sub>O/C catalyst was used in the presence of (CH<sub>3</sub>)<sub>3</sub>COK as a base. The reaction was conducted under a xenon arc lamp with an intensity of 200 mW cm<sup>−2</sup> at 40 °C for six hours. Several protic and aprotic solvents were used to optimize the reaction.

Table 1 Optimization of borylation of aryl halide reaction using Ag–Cu–Cu<sub>2</sub>O/C nanocomposites<sup>a</sup>



Entry	Amount of catalyst	Base	Solvent	t (h)	Yield <sup>b</sup> (%)
1	1 mol%	(CH <sub>3</sub> ) <sub>3</sub> COK	THF	6	51
2	1 mol%	(CH <sub>3</sub> ) <sub>3</sub> COK	Toluene	6	62
3	1 mol%	(CH <sub>3</sub> ) <sub>3</sub> COK	DMF	6	83
4	1 mol%	(CH <sub>3</sub> ) <sub>3</sub> COK	DMSO	6	70
5	1 mol%	(CH <sub>3</sub> ) <sub>3</sub> COK	Methanol	6	42
6	1 mol%	(CH <sub>3</sub> ) <sub>3</sub> COK	Ethanol	6	41
7	1 mol%	(CH <sub>3</sub> ) <sub>3</sub> COK	Dioxane	6	27
8	1 mol%	NaOH	DMF	6	73
9	1 mol%	KOH	DMF	6	75
10	1 mol%	Cs <sub>2</sub> CO <sub>3</sub>	DMF	6	64
11	1 mol%	NaOMe	DMF	6	36
12	2 mol%	(CH <sub>3</sub> ) <sub>3</sub> COK	DMF	6	96
13	3 mol%	(CH <sub>3</sub> ) <sub>3</sub> COK	DMF	6	97
14	2 mol%	(CH <sub>3</sub> ) <sub>3</sub> COK	DMF	3	71
15	2 mol%	(CH <sub>3</sub> ) <sub>3</sub> COK	DMF	1	43

<sup>a</sup> Reaction conditions: 4-iodotoluene (1.2 mmol), bis(pinacolato)diboron (0.6 mmol), catalyst (2 mol%), base (2 equivalent), and xenon arc lamp with the intensity of 200 mW cm<sup>−2</sup>. <sup>b</sup> Yields determined by GC-MS.

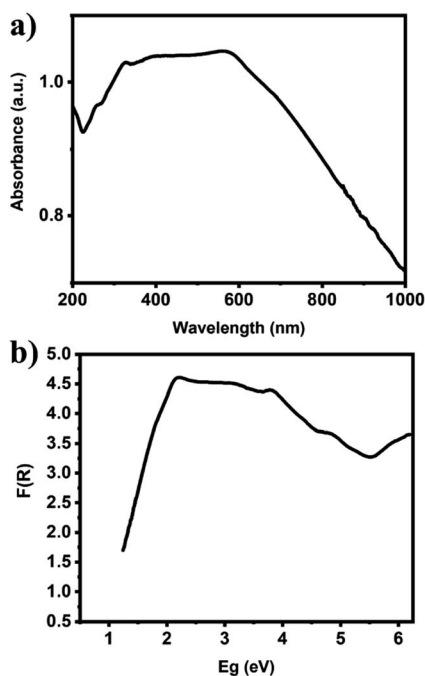


Fig. 5 (a) UV-Vis DRS of Ag–Cu–Cu<sub>2</sub>O/C nanocomposites and (b) the calculated band gap energy of Ag–Cu–Cu<sub>2</sub>O/C nanocomposites.



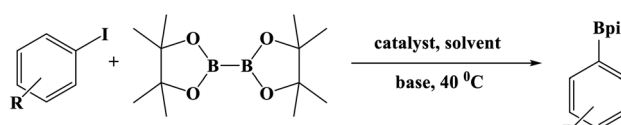
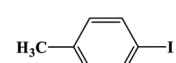
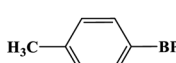
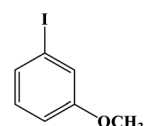
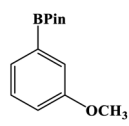
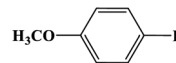
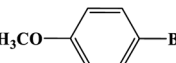
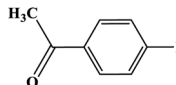
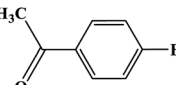
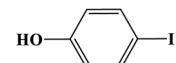
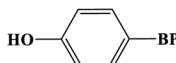
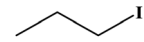
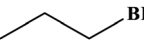
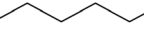
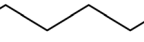
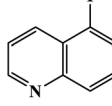
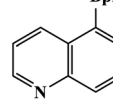
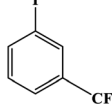
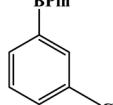
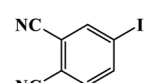
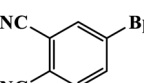
When THF and toluene were used as solvents, low conversions between 51 to 62% were observed (Table 1, entries 1 and 2). Low conversion was also observed when protic solvents, such as methanol (42%) and ethanol (41%), were used (Table 1, entries 5 and 6). The lowest yield (27%) was obtained when dioxane was used (Table 1, entry 7). Good results were obtained when DMF and DMSO were used (83 and 70%, respectively) (Table 1, entries 3 and 4). Therefore, DMF was used as a solvent for further optimization reaction.

Different bases were also used for this reaction. When strong bases, such as NaOH and KOH, were used, the yields decreased

to 73 and 75%, respectively (Table 1, entries 8 and 9). This suggests that a strong base is not effective in this reaction. In addition,  $\text{Cs}_2\text{CO}_3$  could not give a good result with a low yield (64%) (Table 1, entry 10). The lowest yield was afforded when NaOMe was used as a base (36%) (Table 1, entry 11). Thus,  $(\text{CH}_3)_3\text{COK}$  is the best base for this reaction compared to the other bases. The amount of catalyst was also screened. When the catalyst amount was increased to 2 and 3 mol%, the conversion increased to 96 and 97% (Table 1, entries 12 and 13). On the other hand, because there was almost no difference in yield between 2 and 3 mol% of catalyst, 2 mol% of catalyst was used as the optimal amount of catalyst in a further reaction. In addition, the yield also decreases to 71 and 43% when the reaction time was decreased to three and one hour, respectively (Table 1, entries 14 and 15). Thus, the following conditions were used for further experiments: DMF as the solvent,  $(\text{CH}_3)_3\text{COK}$  as the base, 2 mol% catalyst, 40 °C reaction temperature, and six-hour reaction time.

Furthermore, the photocatalytic activity of borylation of aryl halide was screened using various aryl halides under the optimal conditions. Under the optimal conditions, the reactions produced moderate to excellent yields. The methyl group as an electron-donating group at the *para* position of aryl halide afforded a high product yield of 96% (Table 2, entry 1). Another electron-donating group attached to the aryl halide, such as *p*-OH, also resulted in a high yield (93%) (Table 2, entry 5). Electron-withdrawing groups, such as *m*- $\text{OCH}_3$ , *p*- $\text{OCH}_3$ , and *p*- $\text{COCH}_3$ , also showed a high yield of approximately 95, 91, and 94%, respectively (Table 2, entries 2–4). On the other hand, the *m*- $\text{CF}_3$  showed a moderate yield (84%) in this reaction (Table 2, entry 9). The use of iodoalkane groups, such as iodopropane

Table 2 Reactant scope of borylation of aryl halide reaction using Ag–Cu– $\text{Cu}_2\text{O}$ /C nanocomposites<sup>a</sup>

			
Entry	Arylboronic acid	Product	Yield <sup>b</sup> (%)
1			96
2			95
3			91
4			94
5			93
6			98
7			99
8			85
9			84
10			82

<sup>a</sup> Reaction conditions: aryl halide (1.2 mmol), bis(pinacolato)diboron (0.6 mmol), catalyst (2 mol%), base (2 equivalent), and xenon arc lamp with the intensity of 200 mW  $\text{cm}^{-2}$ . <sup>b</sup> Yields determined by GC-MS.

Table 3 The comparison of borylation of aryl halide with other catalysts<sup>a</sup>

Reaction scheme showing the Suzuki-Miyaura cross-coupling of 4-iodotoluene with bis(pinacolato)diboron. The reaction is catalyzed by a catalyst in a solvent at 40 °C in the presence of a base, yielding 4-(pinacolatoboryl)toluene (H<sub>3</sub>C-C<sub>6</sub>H<sub>4</sub>-Bpin).

Entry	Amount of catalyst	Catalyst	Solvent	<i>t</i> (h)	Yield <sup>b</sup> (%)
1	2 mol%	Ag–Cu–Cu <sub>2</sub> O/C	DMF	6	96
2	2 mol%	Cu–BTC	DMF	6	35
3	2 mol%	Cu–Cu <sub>2</sub> O/C	DMF	6	81
4	2 mol%	CuO	DMF	6	38
5	2 mol%	Cu <sub>2</sub> O	DMF	6	43
6	2 mol%	Ag NPS	DMF	6	65
7	2 mol%	Cu NPS	DMF	6	72
8	2 mol%	4 + 5	DMF	6	44
9	2 mol%	6 + 7	DMF	6	77
10	2 mol%	Ag–Cu–Cu <sub>2</sub> O/C	DMF	6	21 <sup>c</sup>
11	—	—	DMF	6	5

<sup>a</sup> Reaction conditions: 4-iodotoluene (1.2 mmol), bis(pinacolato)diboron (0.6 mmol), catalyst (2 mol%), base (2 equivalent), and xenon arc lamp with the intensity of 200 mW  $\text{cm}^{-2}$ . <sup>b</sup> Yields determined by GC-MS. <sup>c</sup> Yield without using light irradiation (dark experiment).



and iodopentane, produced the highest yield of 98 and 99%, respectively (Table 2, entries 6 and 7). The heteroatomic group, such as 6-iodoquinoline, was also used in this reaction, and it showed a moderate yield of 85% (Table 2, entry 8). In addition, two cyanide groups at the *meta* and *para* positions showed moderate conversion with 82% yield (Table 2, entry 10). These results showed that this catalyst could be used for the borylation of various aryl halides under optimal conditions and xenon lamp irradiation.

For comparison, other catalysts were screened for this reaction under optimal conditions. The activity of Cu-BTC was analyzed and showed the lowest yield of 35% (Table 3, entry 2). Similar results also occurred when CuO and Cu<sub>2</sub>O were used as the catalysts for this reaction (38 and 43%) (Table 3, entries 4 and 5). This suggests that these materials are unsuitable for catalyzing the borylation of aryl halides even when a mixture of CuO and Cu<sub>2</sub>O was used (Table 3, entry 8). Moreover, moderate yields were also obtained when single Ag NPS and Cu NPS were used with 65 and 72%, respectively (Table 3, entries 6 and 7). The yield increased moderately when a mixture of Ag and Cu NPS was used (77%) (Table 3, entry 9). Cu-Cu<sub>2</sub>O/C nanoparticles derived from Cu-BTC were also synthesized for comparison using the same method as Ag-Cu-Cu<sub>2</sub>O/C without the addition of Ag. The results showed moderate conversion (81%) (Table 3, entry 3), indicating a synergistic effect between Ag, Cu, Cu<sub>2</sub>O, and C because of the high yield when Ag-Cu-Cu<sub>2</sub>O/C was used as a catalyst (Table 3, entry 1). In addition, the experiments without using light irradiation (dark experiment) and catalyst were conducted with low yields (Table 3, entries 10 and 11). Table 4 compares the borylation of aryl halides using the reported catalysts. The Ag-Cu-Cu<sub>2</sub>O/C nanocomposites had a better catalytic activity with a small amount of catalyst and a short reaction time than the reported catalysts.

The recyclability test of Ag-Cu-Cu<sub>2</sub>O/C nanoparticles was conducted using 4-iodotoluene and bis(pinacolato)diboron under the optimized conditions. The catalyst was separated from the mixture, washed several times with methanol, and collected by centrifugation. The catalyst was dried in a vacuum oven at 80 °C and reused for seven cycles. Fig. 6 shows that the Ag-Cu-Cu<sub>2</sub>O/C nanoparticles have high photocatalytic activity without any significant decrease in photocatalytic activity with a >90% yield. Furthermore, the stability and durability of the nanoparticles were investigated after seven cycles using TEM characterization. After use, the nanoparticles maintained their

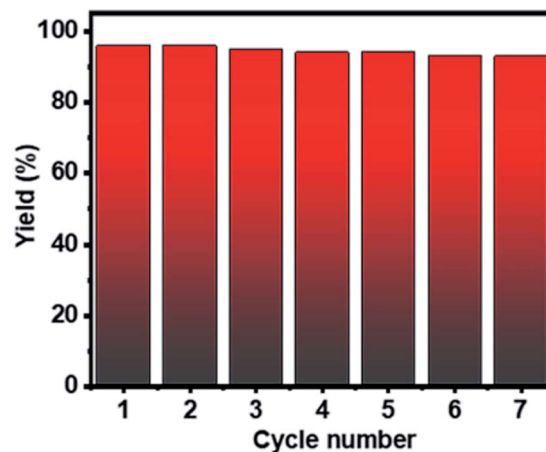


Fig. 6 The recyclability of Ag-Cu-Cu<sub>2</sub>O/C for borylation of aryl halide reaction.

particle size and did not undergo severe particle aggregation (Fig. 7).

The photocatalysis reaction is the catalyst activity in the reaction process induced by UV-Vis light. Through this process, electrons and holes were generated and acted as charge carriers. Generally, photocatalysis using heterogeneous semiconductor catalysts, such as ZnO, CuO, Cu<sub>2</sub>O, and TiO<sub>2</sub>, are promising materials used in many fields.<sup>37–41</sup> Moreover, the addition of metal nanoparticles, such as Ag and Cu, which have surface plasmon resonance (SPR) to absorb visible light, can form a Schottky barrier that suppresses the recombination of photogenerated electron-hole pairs at the interface between the metal and semiconductor.<sup>42–46</sup> Electrons are excited from the valence band to the conduction band when the semiconductor material is excited by UV-Vis light. The excited electrons are transferred to the metal nanoparticles to suppress the recombination of photogenerated electron-hole pairs.<sup>47</sup> This process generates radical species that are used in the borylation of aryl halide reactions. Based on previous studies reported by Mazzearella *et al.* (2019), the borylation of aryl halide reactions under light conditions was exploited in S<sub>N</sub>2-based radical generation.<sup>35</sup> The catalyst can activate aryl halide as electrophile group *via* S<sub>N</sub>2 reaction. Then, aryl halide-catalyst intermediate undergoes the homolytic cleavage of C-X bond due to the light irradiation. Thus, it provides access to alkyl boronate esters to react with the aryl radical to form the product. Therefore, the

Table 4 The comparison of borylation of aryl halide with reported catalysts

Catalyst	Method	Amount of catalyst	Reaction time (h)	Yield (%)	Ref.
Pd(PPh <sub>3</sub> ) <sub>4</sub>	Light irradiation	3 mol%	8	56	33
<i>fac</i> -Ir(ppy) <sub>3</sub>	Light irradiation	2.0 μmol	16	79	34
DTC	Light irradiation	10 mol%	16	95	35
Fe[N(Si(CH <sub>3</sub> ) <sub>3</sub> ) <sub>2</sub> ] <sub>2</sub>	Without light	10 mol%	24	95	36
Cu-Cu <sub>2</sub> O/C	Light irradiation	2 mol%	6	81	This work
Ag-Cu-Cu <sub>2</sub> O/C	Light irradiation	2 mol%	6	96	This work



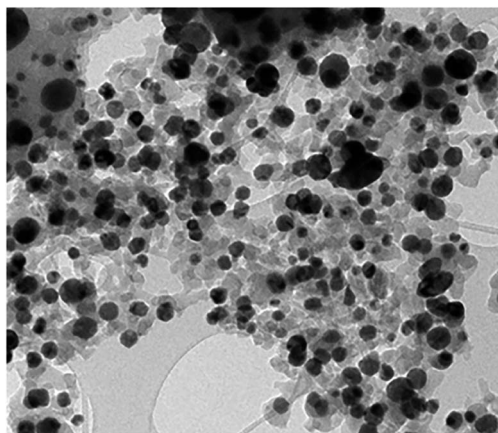


Fig. 7 TEM image of the recovered Ag-Cu-Cu<sub>2</sub>O/C nanoparticles after 7 cycles reaction. The bar represents 100 nm.

formation of radicals from the photogenerated electron-hole pairs of Ag-Cu-Cu<sub>2</sub>O/C nanocomposites is necessary for the borylation of aryl halide reactions.

## Conclusions

Ag-Cu-Cu<sub>2</sub>O/C nanocomposites were prepared *via* one-pot synthesis derived from a metal-organic framework. The high photocatalytic activity was evaluated for the borylation of aryl halide reactions under exposure to a xenon arc lamp with various aryl halide reactants. These nanocomposites could be recycled seven times for the borylation of aryl halide reactions without any significant decrease in product yield or change in particle size.

## Conflicts of interest

There are no conflicts to declare.

## Acknowledgements

This research was supported by Basic Science Research Program through the National Research Foundation of Korea (NRF) funded by the Ministry of Science, ICT & Future Planning (NRF-2020R1I1A3067208). This work was supported by a 2 Year Research Grant of Pusan National University.

## References

- 1 Y. Wang, L. Cai, Y. Li, Y. Tang and C. Xie, *Phys. E*, 2010, **43**, 503–509.
- 2 X. Jiang, X. Zhao, L. Duan, H. Shen, H. Liu, T. Hou and F. Wang, *Ceram. Int.*, 2016, **42**, 15160–15165.
- 3 E. González, J. Arbiol and V. F. Puntes, *Science*, 2011, **334**, 1377–1380.
- 4 I. Choi, S. Chun and Y. K. Chung, *J. Org. Chem.*, 2017, **82**, 12771–12777.
- 5 X. Liu, D. Wang and Y. Li, *Nano Today*, 2012, **7**, 448–466.
- 6 N. Serpone, P. Maruthamuthu, P. Pichat, E. Pelizzetti and H. Hidaka, *J. Photochem. Photobiol., A*, 1995, **85**, 247–255.
- 7 Y. Bessekhoud, D. Robert and J. V. Weber, *Catal. Today*, 2005, **101**, 315–321.
- 8 Y. Bessekhoud, D. Robert and J. V. Weber, *J. Photochem. Photobiol., A*, 2004, **163**, 569–580.
- 9 D. S. Su, G. Wen, S. Wu, F. Peng and R. Schlögl, *Angew. Chem., Int. Ed.*, 2017, **56**, 936–964.
- 10 Q. Xiang, J. Yu and M. Jaroniec, *Chem. Soc. Rev.*, 2012, **41**, 782–796.
- 11 S. Navalon, A. Dhakshinamoorthy, M. Alvaro, M. Antonietti and H. García, *Chem. Soc. Rev.*, 2017, **46**, 4501–4529.
- 12 J. Cai, Y. Li, M. Zhang and Z. Li, *Inorg. Chem.*, 2019, **58**, 7997–8002.
- 13 N. T. S. Phan, K. K. A. Le and T. D. Phan, *Appl. Catal., A*, 2010, **382**, 246–253.
- 14 Z. Hasan and S. H. Jhung, *J. Hazard. Mater.*, 2015, **283**, 329–339.
- 15 Z. Li, Y. Peng, X. Xia, Z. Cao, Y. Deng and B. Tang, *Sci. Rep.*, 2019, **9**, 1–7.
- 16 M. G. Campbell and M. Dincă, *Sensors*, 2017, **17**, 1–11.
- 17 N. Stock and S. Biswas, *Chem. Rev.*, 2012, **112**, 933–969.
- 18 W. Chaikittisilp, K. Ariga and Y. Yamauchi, *J. Mater. Chem. A*, 2013, **1**, 14–19.
- 19 F. Marpaung, M. Kim, J. H. Khan, K. Konstantinov, Y. Yamauchi, M. S. A. Hossain, J. Na and J. Kim, *Chem.-Asian J.*, 2019, **14**, 1331–1343.
- 20 J. Hwang, A. Ejsmont, R. Freund, J. Goscińska, B. V. K. J. Schmidt and S. Wuttke, *Chem. Soc. Rev.*, 2020, **49**, 3348–3422.
- 21 A. K. Kar and R. Srivastava, *Inorg. Chem. Front.*, 2019, **6**, 576–589.
- 22 H. Li, L. Cai, X. Wang and H. Shi, *RSC Adv.*, 2021, **11**, 6383–6394.
- 23 H. Lim, M. Yusuf, S. Song, S. Park and K. H. Park, *RSC Adv.*, 2021, **11**, 8709–8717.
- 24 B. Yu, Y. Zhou, P. Li, W. Tu, P. Li, L. Tang, J. Ye and Z. Zou, *Nanoscale*, 2016, **8**, 11870–11874.
- 25 X. Liu, W. Li, N. Chen, X. Xing, C. Dong and Y. Wang, *RSC Adv.*, 2015, **5**, 34456–34465.
- 26 S. Sarina, E. R. Waclawik and H. Zhu, *Green Chem.*, 2013, **15**, 1814–1833.
- 27 P. C. Trippier and C. McGuigan, *MedChemComm*, 2010, **1**, 183–198.
- 28 Y. Kong, J. Grembecka, M. C. Edler, E. Hamel, S. L. Mooberry, M. Sabat, J. Rieger and M. L. Brown, *Chem. Biol.*, 2005, **12**, 1007–1014.
- 29 S. Senaweera and J. D. Weaver, *J. Am. Chem. Soc.*, 2016, **138**, 2520–2523.
- 30 M. S. Oderinde, M. Frenette, D. W. Robbins, B. Aquila and J. W. Johannes, *J. Am. Chem. Soc.*, 2016, **138**, 1760–1763.
- 31 M. E. Budén, J. F. Guastavino and R. A. Rossi, *Org. Lett.*, 2013, **15**, 1174–1177.
- 32 J. Ruch, A. Aubin, G. Erbland, A. Fortunato and J. P. Goddard, *Chem. Commun.*, 2016, **52**, 2326–2329.
- 33 J. H. Zhao, Z. Z. Zhou, Y. Zhang, X. Su, X. M. Chen and Y. M. Liang, *Org. Biomol. Chem.*, 2020, **18**, 4390–4394.



- 34 M. Jiang, H. Yang and H. Fu, *Org. Lett.*, 2016, **18**, 5248–5251.
- 35 D. Mazzarella, G. Magagnano, B. Schweitzer-Chaput and P. Melchiorre, *ACS Catal.*, 2019, **9**, 5876–5880.
- 36 S. Siddiqui, R. Bhawar and K. Geetharani, *J. Org. Chem.*, 2021, **86**, 1948–1954.
- 37 K. H. Kim and S. K. Ihm, *J. Hazard. Mater.*, 2011, **186**, 16–34.
- 38 F. Zhang, X. Wang, H. Liu, C. Liu, Y. Wan, Y. Long and Z. Cai, *Appl. Sci.*, 2019, **9**, 9–52.
- 39 A. Ajmal, I. Majeed, R. N. Malik, H. Idriss and M. A. Nadeem, *RSC Adv.*, 2014, **4**, 37003–37026.
- 40 S. Chakrabarti and B. K. Dutta, *J. Hazard. Mater.*, 2004, **112**, 269–278.
- 41 F. Han, V. S. R. Kambala, M. Srinivasan, D. Rajarathnam and R. Naidu, *Appl. Catal., A*, 2009, **359**, 25–40.
- 42 E. Mendoza-Mendoza, A. G. Nuñez-Briones, L. A. García-Cerda, R. D. Peralta-Rodríguez and A. J. Montes-Luna, *Ceram. Int.*, 2018, **44**, 6176–6180.
- 43 R. Saravanan, D. Manoj, J. Qin, M. Naushad, F. Gracia, A. F. Lee, M. M. Khan and M. A. Gracia-Pinilla, *Process Saf. Environ. Prot.*, 2018, **120**, 339–347.
- 44 Y. Huang, Z. Liu, G. Gao, G. Xiao, A. Du, S. Bottle, S. Sarina and H. Zhu, *ACS Catal.*, 2017, **7**, 4975–4985.
- 45 Y. Liang, N. Guo, L. Li, R. Li, G. Ji and S. Gan, *New J. Chem.*, 2016, **40**, 1587–1594.
- 46 P. A. Desario, J. J. Pietron, T. H. Brintlinger, M. McEntee, J. F. Parker, O. Baturina, R. M. Stroud and D. R. Rolison, *Nanoscale*, 2017, **9**, 11720–11729.
- 47 K. H. Leong, A. A. Aziz, L. C. Sim, P. Saravanan, M. Jang and D. Bahnemann, *Beilstein J. Nanotechnol.*, 2018, **9**, 628–648.

